Canonical Huynen Decomposition of Radar Targets

Dong Li* and Yunhua Zhang
Key Laboratory of Microwave Remote Sensing, Center for Space Science and Applied Research, Chinese Academy of Sciences, NO. 1 Nanertiao, Zhongguancun, Haidian, Beijing, China 100190

ABSTRACT

Huynen decomposition prefers the world of basic symmetry and regularity (SR) in which we live. However, this preference restricts its applicability to ideal SR scatterer only. As for the complex non-symmetric (NS) and irregular (IR) scatterers such as forest and building, Huynen decomposition fails to analyze their scattering. The canonical Huynen dichotomy is devised to extend Huynen decomposition to the preferences for IR and NS. From the physical realizability conditions of polarimetric scattering description, two other dichotomies of polarimetric radar target are developed, which prefer scattering IR, and NS, respectively, and provide two competent supplements to Huynen decomposition. The canonical Huynen dichotomy is the combination of the two dichotomies and Huynen decomposition. In virtue of an adaptive selection, the canonical Huynen dichotomy is used in target extraction, and the experiments on AIRSAR San Francisco data demonstrate its high efficiency and excellent discrimination of radar targets.

Keywords: Canonical Huynen dichotomy, Huynen-type target dichotomy, target decomposition, scattering preference, phenomenological theory, physical realizability conditions, polarimetric synthetic aperture radar, target extraction

1. INTRODUCTION

Polarimetric target decomposition concept was first formalized by Huynen in his Ph.D. dissertation[1]. Since this work, a great deal of decompositions has been proposed[2]. To classify the terrain by extracting helpful scattering information from PolSAR data via target decomposition has become one of the highly focused topics in geoscience and remote sensing research. It plays an important role in monitoring the natural disasters such as volcano eruption, landslide, earthquake, and tsunami, and inspecting the human activity-related environmental changes such as wetland degradation and deforestation[3, 4].

Although is of theoretical importance, however, Huynen decomposition has not received wide application and attentions. A commonly-recognized reason is the non-uniqueness, because there may theoretically exist infinite target dichotomies if Huynen's restriction on roll-invariance is removed[5]. Nevertheless, in this paper, we do not pay particular attention on such imperfection of Huynen decomposition, because it also exists in other decompositions[6]. Instead, our attention is paid to the incapability of Huynen decomposition on the analysis of irregular and non-symmetric targets. This has been independently assured by Holm and Barnes[7], Yang *et al.*[8], and Paladini[9]. Holm and Barnes found this when they used Huynen decomposition to process a rotated diplane immersed in polarization noise[7]. It was further observed by Yang *et al*. on a distributed dihedral scatterer (entropy is 0.08, alpha angle is 88.93°) [8]. Paladini recently conducted a similar experiment on a distributed ship target dominated by even bounce scattering, and he concluded that "the Huynen theory about the high-frequency noise nature of the *N*-target and the specular nature of the signal part is failed in practice for all such cases where a dominant dihedral scattering is observed" [9].

This paper gives a revisitation to Huynen decomposition. Huynen's preference for scattering symmetry and regularity (SR) is found to be the main reason that restricts the application of Huynen decomposition. From the physical realizability conditions of scattering description, two other target dichotomies are devised, which prefer scattering irregularity (IR) and non-symmetry (NS), respectively. A canonical Huynen dichotomy is developed as the combination of the two dichotomies and Huynen decomposition, and is tested in the application of target extraction. Experiments on the real PolSAR data show its nice performance.

The rest of the paper is arranged as follows. The physical realizability conditions of scattering description are simply formulated in Section 2. Based on which, Huynen decomposition is presented in Section 3 and the canonical Huynen dichotomy is developed in Section 4. Section 5 applies the canonical dichotomy to target extraction. The paper is finally concluded in Section 6.

*lidong@mirslab.cn/lidong108@mails.gucas.ac.cn; phone/fax 86 10 62582874

2. PHYSICAL REALIZABILITY CONDITIONS OF POLARIMETRIC SCATTERING DESCRIPTION

Single target and mixed target represent two different scenarios of target scattering in radar polarimetry. In single target scenario, the target stably scatters the incident wave with no depolarization, and the scattering is then described by the scattering **[*S*]** matrix, which has only five degree of freedoms (DoFs) in monostatic backscattering. As for a mixed target situated in dynamic environment or subjected to spatial/temporal variation, the target scattering is partially polarized and we cannot depict it by a fixed **[*S*]** matrix anymore. The coherence **[*T*]** matrix is then constructed in terms of the statistical average of all the scattering information

$$[\boldsymbol{T}] = \left\langle \boldsymbol{k} \cdot \boldsymbol{k}^{\mathrm{H}} \right\rangle = \begin{bmatrix} 2A_0 & C - jD & H + jG \\ C + jD & B_0 + B & E + jF \\ H - jG & E - jF & B_0 - B \end{bmatrix} \tag{1}$$

where $\langle \cdots \rangle$ is the ensemble average operation, $\boldsymbol{k}$ is the Pauli vector, and the superscript H denotes the operation of conjugate transpose. Ensemble average makes the nine parameters of **[*T*]** mutually independent, a mixed target cannot be directly represented by a single target because of the four more DoFs. The nine parameters on right side are the Huynen parameters, because Huynen first bridged them to the phenomenological characters of radar targets. As illustrated in Figure 1, $2A_0$, B_0+B, and $B_0–B$ are the generators of SR, IR, and NS, respectively, while the others denote the pairwise couplings between the generators[1].

A 3 × 3 complex Hermitian matrix is qualified as a target coherence matrix unless it satisfies the physical realizability conditions. As for a mixed target, the realizability conditions require **[*T*]** be positive semidefinite, and the three 2nd-order principal minors should be nonnegative

$$\text{For mixed target, } \begin{cases} B_0^2 > B^2 + E^2 + F^2 & \text{(-1)} \\ 2A_0\left(B_0 - B\right) > H^2 + G^2 & \text{(-2)} \\ 2A_0\left(B_0 + B\right) > C^2 + D^2 & \text{(-3)} \end{cases}. \tag{2}$$

In the single target scenario, **[*T*]** is rank-one and all the 2nd-order minors should be zero. Nine equations are then obtained, but only four of them are independent because single target has five DoFs. We can therefore extract the following three condition groups:

$$\begin{cases} 2A_0\left(B_0 - B\right) = H^2 + G^2 \\ 2A_0\left(B_0 + B\right) = C^2 + D^2 \\ 2A_0\left(E + jF\right) = \left(C + jD\right)\left(H + jG\right) \end{cases} \text{(-1)} \qquad \begin{cases} \left(B_0 + B\right) \cdot 2A_0 = C^2 + D^2 \\ \left(B_0 + B\right)\left(B_0 - B\right) = E^2 + F^2 \\ \left(B_0 + B\right)\left(H + jG\right) = \left(C - jD\right)\left(E + jF\right) \end{cases} \text{(-2)}$$

$$\begin{cases} \left(B_0 - B\right) \cdot 2A_0 = H^2 + G^2 \\ \left(B_0 - B\right)\left(B_0 + B\right) = E^2 + F^2 \\ \left(B_0 - B\right)\left(C - jD\right) = \left(H + jG\right)\left(E - jF\right) \end{cases} \text{(-3).} \tag{3}$$

Each group of (3) is self-contained and from them we can get the following three equations, respectively

$$\text{For single target, } \begin{cases} B_0^2 = B^2 + E^2 + F^2 & \text{(-1)} \\ 2A_0\left(B_0 - B\right) = H^2 + G^2 & \text{(-2)} \\ 2A_0\left(B_0 + B\right) = C^2 + D^2 & \text{(-3)} \end{cases}. \tag{4}$$

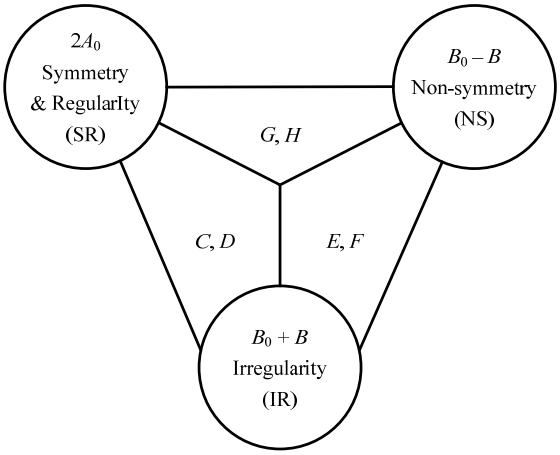

Figure 1. Phenomenological significance of the nine Huynen parameters.

3. HUYNEN DECOMPOSITION

The same four parameters such as (B_0, B, E, F) behave differently in the two target scenarios, being similar to the behavior of the four Stokes parameters in the two wave scenarios of full polarization and partial polarization. Wave dichotomy theorem declares that we can always decompose a partially polarized wave into the sum of a fully polarized wave and a fully depolarized wave[2]. By analogy, Huynen developed a target dichotomy to write a mixed target $\mathbf{[}\boldsymbol{T}\mathbf{]}$ into the sum of an equivalent single target $\mathbf{[}\boldsymbol{T}_{\boldsymbol{S1}}\mathbf{]}$ and a noisy N-target $\mathbf{[}\boldsymbol{T}_{\boldsymbol{N1}}\mathbf{]}$. Huynen insisted that the real world physically prefers SR and the related parameters ($2A_0$, C, D, G, H) should be preserved into the single target, therefore, he chose to decompose parameters (B_0, B, E, F) only [1]

$$\left[\boldsymbol{T}\right]=\left[\boldsymbol{T}_{\boldsymbol{S1}}\right]+\left[\boldsymbol{T}_{\boldsymbol{N1}}\right]=\begin{bmatrix} 2A_0 & C-jD & H+jG \\ C+jD & B_{0S}+B_S & E_S+jF_S \\ H-jG & E_S-jF_S & B_{0S}-B_S \end{bmatrix}+\begin{bmatrix} 0 & 0 & 0 \\ 0 & B_{0N}+B_N & E_N+jF_N \\ 0 & E_N-jF_N & B_{0N}-B_N \end{bmatrix}. \tag{5}$$

The subscripts S and N index the equivalent single target and N-target, respectively. If we replace (B_0, B, E, F) with (B_{0S}, B_S, E_S, F_S), then parameters (B_{0S}, B_S, E_S, F_S) can be inverted from (3-1) based on the preserved parameters ($2A_0$, C, D, G, H).

4. CANONICAL HUYNEN DICHOTOMY

Huynen reserved the SR-related parameters into $\mathbf{[}\boldsymbol{T}_{\boldsymbol{S1}}\mathbf{]}$ because it "leads to a consistent world-picture where psychological preference for symmetry" [1]. This kind of world view restricts the applicability of Huynen decomposition to ideal SR target only, i.e. it fails to analyze the complex IR and NS targets. This has been validated by Holm and Barnes[7], Yang *et al.*[8], and Paladini[9]. As a response, Huynen pointed out, our attention should turn from $\mathbf{[}\boldsymbol{T}_{\boldsymbol{S1}}\mathbf{]}$ to $\mathbf{[}\boldsymbol{T}_{\boldsymbol{N1}}\mathbf{]}$ in these cases[10]. However, we can observe from (5) that the IR- and NS-related parameters (B_0, B, E, F) are distributed into both $\mathbf{[}\boldsymbol{T}_{\boldsymbol{N1}}\mathbf{]}$ and $\mathbf{[}\boldsymbol{T}_{\boldsymbol{S1}}\mathbf{]}$, thus the attention on $\mathbf{[}\boldsymbol{T}_{\boldsymbol{S1}}\mathbf{]}$ or $\mathbf{[}\boldsymbol{T}_{\boldsymbol{N1}}\mathbf{]}$ is all inappropriate for the integrated characterization of such radar targets.

The canonical Huynen dichotomy is devised to extend Huynen decomposition to the preferences for IR and NS. This in fact can be easily achieved because we still have two mixed target inequations in (2) with their corresponding single target equations appearing in (4). As for parameters ($2A_0$, B_0–B, H, G), if we define

$$B_0' - B' = 2A_0, 2A_0' = B_0 + B, B_0' + B' = B_0 - B \tag{6}$$

which enables us to write (2-2) and (4-2) into the similar forms to (2-1) and (4-1), respectively

$$\begin{cases} B_0'^2 = B'^2 + H^2 + G^2 & \text{for single target} \\ B_0'^2 > B'^2 + H^2 + G^2 & \text{for mixed target} \end{cases}. \tag{7}$$

Analogous to Huynen decomposition, we then have

$$[\boldsymbol{T}] = [\boldsymbol{T_{S2}}] + [\boldsymbol{T_{N2}}] = \begin{bmatrix} 2A_{0S} & C - jD & H_S + jG_S \\ C + jD & B_0 + B & E + jF \\ H_S - jG_S & E - jF & B_{0S} - B_S \end{bmatrix} + \begin{bmatrix} 2A_{0N} & 0 & H_N + jG_N \\ 0 & 0 & 0 \\ H_N - jG_N & 0 & B_{0N} - B_N \end{bmatrix}. \tag{8}$$

Dichotomy (8) prefers IR because it preserves the IR-related Huynen parameters (B_0+B, C, D, E, F) into the matrix of single target. Based on these preserved parameters, the decomposed parameters ($2A_{0S}$, B_{0S}–B_S, G_S, H_S) can be easily retrieved from (3-2).

Likewise, as for parameters ($2A_0$, B_0+B, C, D), if we define

$$B_0'' - B'' = 2A_0, B_0'' + B'' = B_0 + B, 2A_0'' = B_0 - B \tag{9}$$

from (2-3) and (4-3) we then have

$$\begin{cases} B_0''^2 = B''^2 + C^2 + D^2 & \text{for single target} \\ B_0''^2 > B''^2 + C^2 + D^2 & \text{for mixed target} \end{cases}. \tag{10}$$

Hence we can also obtain the following target dichotomy:

$$[\boldsymbol{T}] = [\boldsymbol{T_{S3}}] + [\boldsymbol{T_{N3}}] = \begin{bmatrix} 2A_{0S} & C_S - jD_S & H + jG \\ C_S + jD_S & B_{0S} + B_S & E + jF \\ H - jG & E - jF & B_0 - B \end{bmatrix} + \begin{bmatrix} 2A_{0N} & C_N - jD_N & 0 \\ C_N + jD_N & B_{0N} + B_N & 0 \\ 0 & 0 & 0 \end{bmatrix}. \tag{11}$$

Dichotomy (11) prefers NS because it preserves the NS-related parameters (B_0–B, E, F, G, H) into the single target coherence matrix $\boldsymbol{[T_{S3}]}$. Then parameters ($2A_{0S}$, B_{0S}+B_S, C_S, D_S) can be obtained from (3-3) based on the preserved parameters.

Dichotomies (8) and (11) provide two competent supplements to Huynen decomposition. Together with Huynen decomposition, we now obtain three dichotomies preferring SR, IR, and NS, respectively. We term them as the canonical Huynen dichotomy, because Huynen has claimed the existences of $\boldsymbol{[T_{N2}]}$ and $\boldsymbol{[T_{N3}]}$ of dichotomies (8) and (11). They were named the type I and type II symmetrical canonical targets, but were abandoned by Huynen for "having no such natural appeal" like $\boldsymbol{[T_{N1}]}$ [1].

5. EXTRACTION OF DOMINANT TARGET SCATTERING

A single target is a deterministic scatterer and we can easily determine its scattering mechanism. However, a mixed target is a random scatterer which cannot be directly characterized like the single target. Huynen[1] and Cloude[5] proposed to use an equivalent dominant single target to model the scattering of mixed target, but common consciousness has not been achieved in the definition of dominant single target. In Huynen decomposition, it refers to a scatterer which can physically preserve the whole SR information of mixed target. But in eigenvector-based Cloude decomposition, it is a scatterer which can mathematically approximate the mixed target to the most

$$[\boldsymbol{T_{Scd}}] = \boldsymbol{k_{Scd}} \cdot \boldsymbol{k_{Scd}}^{\mathrm{H}} = \lambda_1 \boldsymbol{u}_1 \cdot \boldsymbol{u}_1^{\mathrm{H}}, \text{ and } \boldsymbol{k_{Scd}} = \sqrt{\lambda_1}\boldsymbol{u}_1 \tag{12}$$

where $\boldsymbol{[T_{Scd}]}$ is the extracted dominant scattering with the Pauli vector $\boldsymbol{k_{Scd}}$. It relates to the largest eigenvalue λ_1 and eigenvector $\boldsymbol{u_1}$ of $\boldsymbol{[T]}$. The SPAN of $\boldsymbol{[T_{Scd}]}$ is the largest among all the possible estimations of the dominant scattering of $\boldsymbol{[T]}$ [5].

Table 1. Total power (SPAN) of the dominant single targets extracted by the Cloude decomposition, the canonical Huynen dichotomy, as well as the dichotomies (5), (8), and (11) from the selected three pixel patches.

Patches	SPAN of $[T_{Scd}]$	SPAN of $[T_{Schd}]$	SPAN of $[T_{S1}]$	SPAN of $[T_{S2}]$	SPAN of $[T_{S3}]$
# 1	0.9695	0.9686	**0.9686**	0.7005	0.3461
# 2	0.6169	0.6084	0.3407	**0.6084**	0.1065
# 3	0.4216	0.4019	0.3239	0.2918	**0.4019**

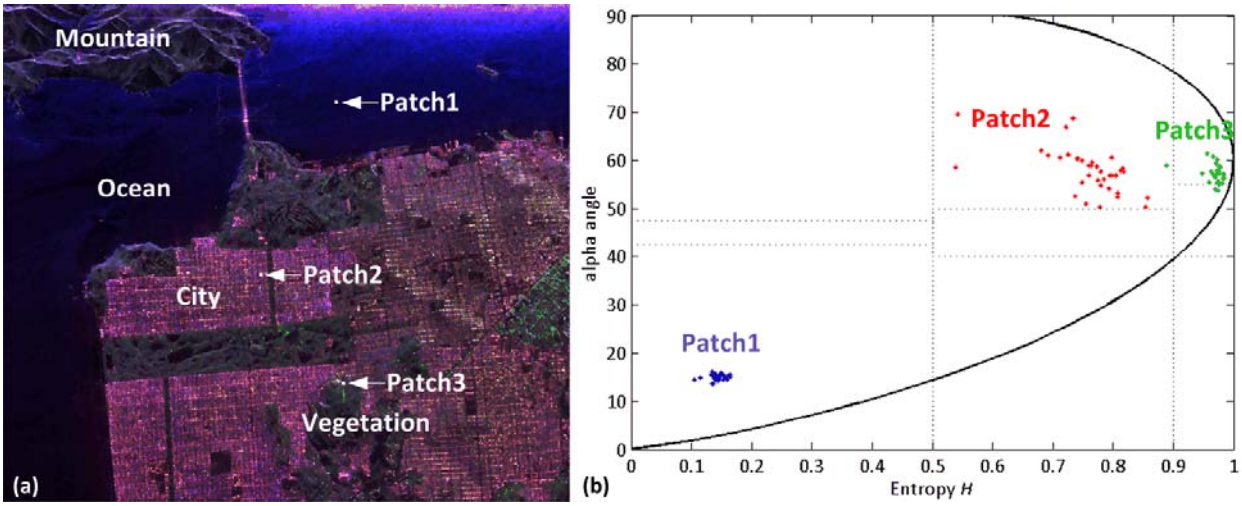

Figure 2. Illustration of the experimental PolSAR data. (a) Pauli display of the L-band AIRSAR San Francisco data, where Patch1, Patch2, and Patch3 are three 6 × 6 pixel patches selected from the areas of ocean, city, and vegetation, respectively. They are used as numerical example, and (b) is their projection in the 2D entropy/alpha classification plane.

As an extension of Huynen decomposition, canonical Huynen dichotomy enables three dichotomies preferring SR, IR, and NS, respectively. By devising a good strategy so that each of the three dichotomies has fair chance of selection, the canonical dichotomy will be used in the adaptive extraction of dominant scattering. Referring to Cloude decomposition, our selection is also based on SPAN, i.e. use the three dichotomies to extract single targets $[T_{S1}]$, $[T_{S2}]$, and $[T_{S3}]$ from mixed target $[T]$, then identify the one with the maximum SPAN as the final dominant single target extraction $[T_{Schd}]$

$$[T_{Schd}] = \sum_{i=1}^{3} c_i [T_{Si}] \tag{13}$$

where c_i (i = 1, 2, 3) is a constant and

$$c_i = \begin{cases} 1, \text{ if } SPAN([T_{Si}]) > SPAN([T_{Sj}]), \ j = 1,2,3, \ j \neq i \\ 0, \text{ else} \end{cases} \tag{14}$$

where $SPAN$ ($[T_{Si}]$) denotes the SPAN of matrix $[T_{Si}]$.

The performance of canonical Huynen dichotomy on dominant scattering extraction is tested on the NASA/JPL L-band AIRSAR data of San Francisco. Figure 2 (a) illustrates the Pauli image of this scene, which covers a variety of scatterers, such as ocean, city, and vegetation. Three 6 × 6 pixel patches are respectively selected from the areas of ocean, city, and vegetation, and their projection in the 2D entropy/alpha classification plane is shown in Figure 2 (b). The three patches correspond to the low-entropy Bragg scattering, medium-entropy dihedral scattering, and high-entropy volume scattering, respectively. As for each patch, we average the $[T]$ matrices of all the 36 pixels in it and normalize the averaged $[T]$

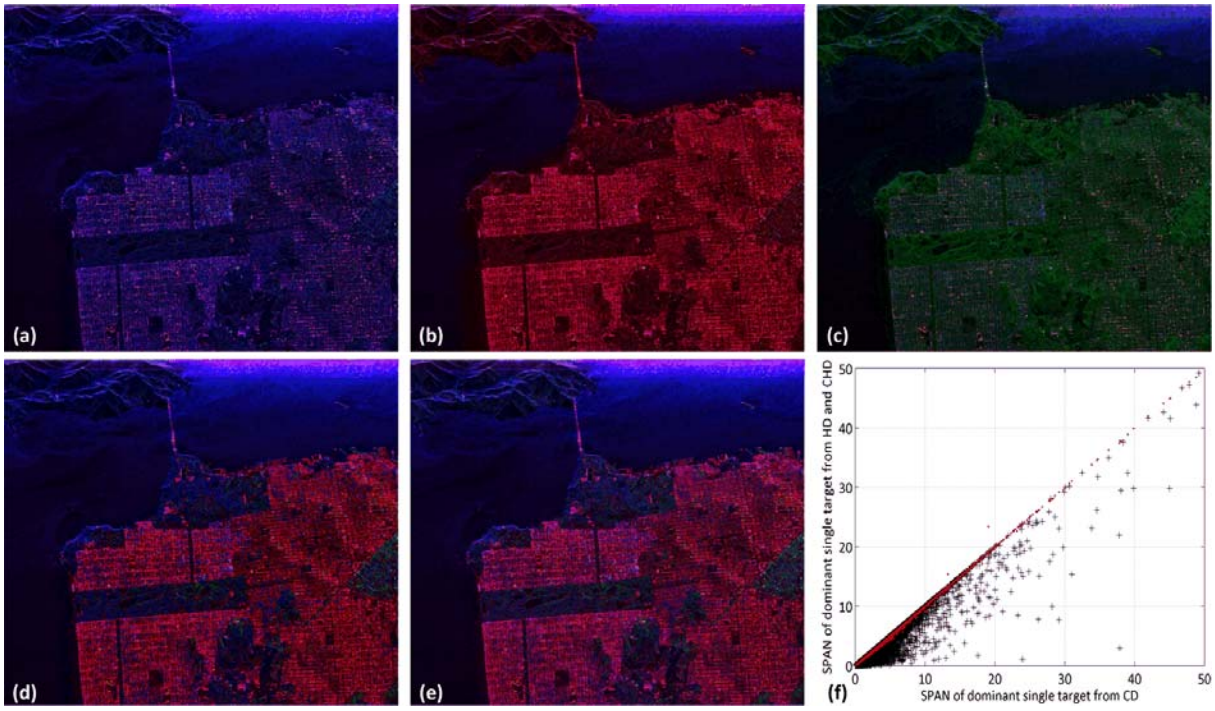

Figure 3. Dominant single target extensions on L-band AIRSAR data of San Francisco. (a) to (e) respectively shows the Pauli image of the dominant single targets $[\boldsymbol{T}_{S1}]$, $[\boldsymbol{T}_{S2}]$, $[\boldsymbol{T}_{S3}]$, $[\boldsymbol{T}_{Schd}]$, and $[\boldsymbol{T}_{Scd}]$ extracted by dichotomy (5) (Huynen decomposition), dichotomy (8), dichotomy (11), canonical Huynen dichotomy, and Cloude decomposition. (f) shows (red point) the relation between *SPAN* ($[\boldsymbol{T}_{Schd}]$) and *SPAN* ($[\boldsymbol{T}_{Scd}]$), as well as (black cross) that between *SPAN* ($[\boldsymbol{T}_{S1}]$) and *SPAN* ($[\boldsymbol{T}_{Scd}]$).

matrix with its trace. Then dichotomies (5), (8), and (11) are applied to extracting the single target scattering from the three normalized mean patches. Table 1 lists the obtained *SPAN* ($[\boldsymbol{T}_{Si}]$) on each patch, and *SPAN* ($[\boldsymbol{T}_{Scd}]$) from Cloude decomposition is also listed for comparison. As we expected, dichotomy (5), i.e. Huynen decomposition behaves the best on Patch1 due to the preference for SR scattering. But on Patch2 and Patch3 where the surface scattering is no longer dominant, Huynen decomposition cannot obtain the satisfactory target extraction, and the majority of power is then decomposed into $[\boldsymbol{T}_{N1}]$. This is consistent with the findings of Holm and Barnes, Yang *et al*., and Paladini. Nevertheless, dichotomies (8) and (11) provide two competent supplements to Huynen decomposition. The single target extracted by dichotomy (8) on Patch 2 reserves the most power. The distributed dihedral scatterer used by Holm and Barnes, Yang *et al*., and Paladini to illustrate the invalidation of Huynen decomposition, however, can be successfully tackled by this dichotomy. Patch3 corresponds to high-entropy volume scattering. Dichotomy (11) behaves the best on this patch among the three dichotomies. Nevertheless, about 60% of the power is still distributed into $[\boldsymbol{T}_{N3}]$. This cannot indicate the bad performance of dichotomy (11), because $[\boldsymbol{T}_{Scd}]$ extracted by Cloude decomposition on this patch also represents only 42.16% of power. The main influence arises from the scattering randomness. The entropy of Patch3 is 0.9838, which signifies the high randomness and nearly isotropic scattering preference. Hence, we cannot identify a prominently strong preferred single target from it. The canonical dichotomy extracts $[\boldsymbol{T}_{Schd}]$ by maximizing the SPAN, as listed in Table 1, *SPAN* ($[\boldsymbol{T}_{Schd}]$) has tiny difference from *SPAN* ($[\boldsymbol{T}_{Scd}]$) on the three patches.

The numerical example above illustrates the scattering preferences of the tree dichotomies on the three selected patches. Dichotomies (5), (8), and (11) intactly reserve the 1st, 2nd, and 3rd columns of $[\boldsymbol{T}]$ into $[\boldsymbol{T}_{S1}]$, $[\boldsymbol{T}_{S2}]$, and $[\boldsymbol{T}_{S3}]$, respectively. We treat this reservation as certain scattering preference and describe the scattering preference of the three dichotomies in terms of the three phenomenological characters. As indicated in Sections 3 and 4, the three dichotomies prefer SR, IR, and NS, respectively, because the three columns of $[\boldsymbol{T}]$ relate to SR, IR, and NS, respectively. Figure 3 (a), (b) and (c) further exhibit the Pauli images of $[\boldsymbol{T}_{S1}]$, $[\boldsymbol{T}_{S2}]$, and $[\boldsymbol{T}_{S3}]$ extracted on the whole scene of San Francisco, respectively.

The dark blue in ocean area of Figure 3 (a) reveals the preference of Huynen decomposition for SR scattering. The wide distribution of red color in Figure 3 (b) indicates the preference of dichotomy (9) for IR dihedral scattering. This dichotomy is thus useful for building detection because buildings generally contribute to the strongest dihedral scattering in urban area. Dichotomy (11) prefers NS volume scattering, and the green forests in Figure 3 (c) clearly reflect this, thus it may be used for forest detection. The three dichotomies provide three different points of view of the mixed targets. Canonical dichotomy combines them into a whole based on the adaptive selection, and the extracted dominant scattering $[\boldsymbol{T}_{Schd}]$ is shown in Figure 3 (d), which looks much closer to the original mixed scattering $[\boldsymbol{T}]$ than $[\boldsymbol{T}_{Si}]$. Furthermore, by adaptively filtering out the unwanted noisy scatterings, canonical dichotomy makes the target scattering signature much clear. The target scattering in Figure 3 (d) is strengthened because the "blur cover" in Figure 2 (a) is removed. This improves the capability for target identification. By counting the contribution of Huynen decomposition to the dominant scattering extraction, 37% of the San Francisco scene is found inappropriate for Huynen decomposition. This validates the restricted application of Huynen decomposition in a sense.

The numerical example above reveals the tiny difference between *SPAN* ($[\boldsymbol{T}_{Schd}]$) and *SPAN* ($[\boldsymbol{T}_{Scd}]$) on the three selected patches. Figure 3 (e) further exhibits the Pauli image of $[\boldsymbol{T}_{Scd}]$ on the whole San Francisco scene, it looks nearly the same as Figure 3 (d). Figure 3 (f) illustrates the relationship between *SPAN* ($[\boldsymbol{T}_{Schd}]$) and *SPAN* ($[\boldsymbol{T}_{Scd}]$), and the nearly linear correlationship indicates their good consistency. As a comparison, Figure 3 (f) also gives the relationship between *SPAN* ($[\boldsymbol{T}_{S1}]$) and *SPAN* ($[\boldsymbol{T}_{Scd}]$). It can be clearly observed that, from the mathematical aspects of target extraction, Huynen decomposition is greatly improved by the canonical dichotomy. The mean relative residue between *SPAN* ($[\boldsymbol{T}_{Schd}]$) and *SPAN* ($[\boldsymbol{T}_{Scd}]$) is only 3.61% on San Francisco scene, but this parameter changes to 14.03% if we replace $[\boldsymbol{T}_{Schd}]$ with $[\boldsymbol{T}_{S1}]$. All these not only demonstrate the superiority of canonical dichotomy over Huynen decomposition, but also show the potential unifiability of canonical dichotomy and Cloude decomposition.

The target extraction in (13) can be equivalently formulated in terms of the Pauli vectors

$$\boldsymbol{k}_{Schd} = \sum_{i=1}^{3} c_i \boldsymbol{k}_{Si} \tag{15}$$

where $\boldsymbol{k}_{Schd}$ and $\boldsymbol{k}_{Si}$ are the Pauli vectors of $[\boldsymbol{T}_{Schd}]$ and $[\boldsymbol{T}_{Si}]$. We can easily obtain from (5), (8), and (11) that

$$\boldsymbol{k}_{S1} = \frac{1}{\sqrt{2A_0}} \begin{bmatrix} 2A_0 \\ C + jD \\ H - jG \end{bmatrix}, \boldsymbol{k}_{S2} = \frac{1}{\sqrt{B_0 + B}} \begin{bmatrix} C - jD \\ B_0 + B \\ E - jF \end{bmatrix}, \boldsymbol{k}_{S3} = \frac{1}{\sqrt{B_0 - B_0}} \begin{bmatrix} H + jG \\ E + jF \\ B_0 - B \end{bmatrix}. \tag{16}$$

Pauli vector $\boldsymbol{k}_{Si}$ directly relates to each column of matrix $[\boldsymbol{T}]$. Therefore, although canonical dichotomy does not seem as straightforward as Cloude decomposition because it needs to perform three dichotomies for the optimum, actually, it can be fast achieved. On the contrary, Cloude decomposition is not so straightforward because it needs to conduct a series of unitary transforms on $[\boldsymbol{T}]$ for the eigenvalue and eigenvector. Although we can accelerate its computation using the LAPACK-based eigenanalysis tool, the resulted computational load is still heavy. To illustrate this, we execute the Matlab codes of the two decompositions on the whole scene of San Francisco 100 times within a computer hardware environment of Pentium (R) 8.00 GB memory and 3.20 GHz CPU clock. The average computational times are 0.2120s and 9.7406s, respectively, and the canonical dichotomy is about 46 times faster than Cloude decomposition.

6. CONCLUSION

The preference for scattering SR restricts the application of Huynen decomposition. The canonical Huynen dichotomy is devised to extend Huynen decomposition to the preferences for IR and NS. A 3 × 3 complex Hermitian matrix is qualified as a polarimetric coherence matrix unless it satisfies the physical realizability conditions. These conditions lay the foundation of the canonical dichotomy. The canonical dichotomy can achieve consistent dominant target extraction as Cloude decomposition, and is more efficient.

ACKNOWLEDGEMENTS

This work was supported in part by the National Natural Science Foundation of China under Grant 41401406 and by the Youth Innovation Promotion Association of Chinese Academy of Sciences under Grant 2014131. The authors would like to thank the National Aeronautics and Space Administration/Jet Propulsion Laboratory for providing the AIRSAR San Francisco data.

REFERENCES

[1] Huynen J. R., [Phenomenological Theory of Radar Targets], Drukkerij Bronder-Offset N.V., Rotterdam, The Netherland, 157-181 (1970).
[2] Lee J.-S. and Pottier E., [Polarimetric Radar Imaging: From Basics to Applications], CRC Press, Boca Raton, FL, USA, 179-264 (2009).
[3] Touzi R., Deschamps A. and Rother G., "Phase of target scattering for wetland characterization using polarimetric C-band SAR," IEEE Trans. Geosci. Remote Sens. 47(9), 3241-3261 (2009).
[4] Yamaguchi Y., "Disaster monitoring by fully polarimetric SAR data acquired with ALOS-PALSAR," Proc. IEEE 100(10), 2851-2860 (2012).
[5] Cloude S. R., "Uniqueness of target decomposition theorems in radar polarimetry," Direct and Inverse Methods in Radar polarimetry, 267-296 (1992).
[6] Cloude S. R., Gil J. J., San Jose I. and Ossikovski R., "Generalized target decomposition theory," Proc. POLINSAR, 1-8 (2013).
[7] Holm W. A. and Barnes R. M., "On radar polarization mixed target state decomposition techniques," Proc. IEEE 1988 National Radar Conf., 249-254 (1988).
[8] Yang J., Peng Y.-N., Yamaguchi Y. and Yamada H., "On Huynen's decomposition of a Kennaugh matrix," IEEE Geosci. Remote Sens. Lett. 3(3), 369-372 (2006).
[9] Paladini R., [Polarimetric Radar Target Decomposition and Classification], Univ. Pisa, Pisa, Italy, 51-55 (2011).
[10] Huynen J. R., "Comments on target decomposition theorems," Direct and Inverse Methods in Radar polarimetry, 387-399 (1992).